Electrical characterization of a large-area single-layer Cu3BHT 2D conjugated coordination polymer

Sandra M. Estévez, Zhiyong Wang, Tsai-Jung Liu, Gabriel Caballero, Fernando J. Urbanos, Ignacio Figueruelo-Campanero, Julia García-Pérez, Cristina Navío, Miroslav Polozij, Jianjun Zhang, Thomas Heine, Mariela Menghini, Daniel Granados, Xinliang Feng, Renhao Dong, Enrique Cánovas

Electrical characterization of a large-area single-layer Cu_3BHT 2D conjugated coordination polymer

Sandra. M. Estévez[a,b,#], Zhiyong Wang[d,e,#], Tsai-Jung Liu[e], Gabriel Caballero[a,c], Fernando J. Urbanos[a], Ignacio Figueruelo-Campanero[a,c], Julia García-Pérez[a], Cristina Navío[a], Miroslav Polozij[e,f,g], Jianjun Zhang[e], Thomas Heine[e,f,g,h], Mariela Menghini[a] , Daniel Granados[a], Xiliang Feng[d,e,*], Renhao Dong[i,j,*], and Enrique Cánovas[a,*].

[a] *IMDEA Nanociencia, 28049 Madrid, Spain.*

[b] *Escuela de Doctorado, Universidad Autónoma de Madrid, 28049 Madrid, Spain.*

[c] *Facultad Ciencias Físicas, Universidad Complutense de Madrid, 28040 Madrid, Spain*

[d] *Max Planck Institute of Microstructure Physics, Halle (Saale), Germany.*

[e] *Center for Advancing Electronics Dresden (cfaed) & Faculty of Chemistry and Food Chemistry, Technische Universität Dresden, Germany.*

[f] *Helmholtz-Zentrum Dresden-Rossendorf (HZDR), Abteiling Ressoursenökilogie, 04318 Leipzig, Germany.*

[g] *Center for Advanced Systems Understanding, CASUS, Untermarkt 20, 02826 Görlitz, Germany.*

[h] *Department of Chemistry, Yonsei University, Seodaemun-gu, Seoul, 120-749 Republic of Korea.*

[i] *Key Laboratory of Colloid and Interface Chemistry of the Ministry of Education, School of Chemistry and Chemical Engineering, Shandong University, Jinan, 250199 China.*

[j] *Materials Innovation Institute for Life Sciences and Energy (MILES) & Department of Chemistry, University of Hong Kong, China.*

[#] These authors contributed equally

[*] Author to whom correspondence should be addressed: xinliang.feng@tu-dresden.de, renhaodong@sdu.edu.cn, enrique.canovas@imdea.org

Abstract

Understanding charge transport properties of large-area single-layer 2D materials is crucial for the future development of optoelectronic devices. In this work, we report the synthesis and electrical characterization of a large-area single-layer of Cu_3BHT two-dimensional conjugated coordination polymer. The Cu_3BHT was synthesized on the water surface by the Langmuir-Blodgett method and then transferred to SiO_2/Si substrates with pre-patterned electrical contacts. Electrical measurements revealed ohmic responses across areas up to ~1 cm^2, with a mean resistance of approximately 53 ± 3 kΩ at a probe separation of 50 μm. Cooling and heating cycles showed hysteresis in the electrical response, suggesting different current pathways are formed as the samples underwent structural-chemical changes during temperature sweeps. This hysteresis vanished after several cycles and the conductivity showed a stable exponential behavior as a function of temperature, suggesting that a temperature-dependent tunneling process was governing the conduction mechanism in the analyzed polycrystalline single-layer Cu_3BHT samples. These results, together with density functional theory calculations and valence band X-

ray photoelectron spectroscopy data suggest that the single-layer samples exhibit a semiconducting rather than a metallic behavior.

Keywords: *Cu_3BHT, 2D coordination polymer, 2D metal-organic framework, single-layer, electrical resistivity, electrical conductivity, contact resistance, semiconductor.*

Introduction

Two-dimensional conjugated coordination polymers (2D c-CPs), including 2D conjugated metal-organic frameworks (2D c-MOFs), are crystalline materials characterized by strong π-d conjugation [1][2]. These materials are formed by the coordination of metal centers and planar organic conjugated building blocks [3]. Unlike traditional 2D materials derived from bulk crystal exfoliation, the modular nature of 2D c-MOFs affords tailorable structures and chemistry at the molecular level, making them highly advantageous for realizing materials with extensive tunability of their electrical properties [3]. Among all available c-MOFs, the sub-family of 2D MOFs are at the forefront in displaying high electrical conductivities [4-8]; this singularity has made this type of materials suitable as active and passive elements in optoelectronics [9]. A notable example is Cu_3BHT, which has displayed record room temperature conductivities up to ~2500 Scm^{-1} [8][10]. This performance has been attributed to a lack of in-plane porosity, enabling dense packing of Cu ions and BHT ligands in a Kagome-like lattice, which contributes to significant hybridization of the π (BHT ligands)-d (Cu ions) orbitals [10]. However, most reports on 2D c-CPs or c-MOFs, and specifically on Cu_3BHT, refer to studies of layer-stacked samples, where highly delocalized electrons are expected along both in-plane and out-of-plane crystal directions in van der Waals layer-stacked structures [2][7][11]. In this respect, it is worth noting that the electrical properties of isolated single-layer Cu_3BHT samples remain unexplored. In order to add 2D c-CPs to the library of currently available 2D materials, it is then critical to realize large-area single-layer samples and reliably characterize their electrical properties.

In this work, we report on the preparation of large-area polycrystalline Cu_3BHT single-layers, which provide a platform for exploring charge transport in the 2D limit in this material. Single-layers of Cu_3BHT with a lateral size up to ~50 cm^2 and thicknesses of 0.8 nm were synthesized by on-water surface chemistry. Using diffraction and imaging techniques, we resolved the Kagome structure of single-layer Cu_3BHT with atomic resolution. The single-layer samples were deposited onto Au pre-patterned silicon substrates containing several device configurations for electrical characterization. First, we mapped the electrical resistance to study the homogeneity of the sample across ~1 cm^2 area and found ohmic responses with a mean value of 53.29 kΩ and a maximum deviation of 6% for devices with a channel length of 50 μm. By means of the transfer

length method a contact resistance of 20.7 ± 1.5 kΩ was found, consistent with the sample´s resistance over 50 μm channel lengths. The temperature dependence of the resistivity of single-layer Cu_3BHT was analyzed using the 4-probe method, showing a notable hysteresis between cooling and warming curves, more pronounced below 150 K. After several cycles, the hysteresis settled, indicating most likely the stabilization of a charge conduction percolation path across the 2D polycrystalline sample. The resistivity increased with decreasing temperature, displaying a semiconductor-like response. The conductivity vs temperature analysis showed that a singular exponential dependence of σ vs temperature modeled the data over the wider temperature range. A result in agreement with the one found for a temperature-dependent tunneling process in low-mobility semiconductors [12]. This observation suggests that long-range charge transport is limited by a temperature-activated process at the grain boundaries of the polycrystalline Cu_3BHT sample. Theoretical calculations revealed a stable wavy structure for the Cu_3BHT single-layer, potentially induced by water adsorption, which exhibits a semiconducting, rather than metallic, nature. These results, together with Valence Band X-ray Photoelectron Spectroscopy (VB XPS) characterization support the semiconducting nature of the obtained single-layer Cu_3BHT samples. This work lays the foundation for a reliable characterization of single-layer organic and organo-metallic materials, contributing to a deeper understanding of the interplay between chemistry, structure, and macroscopic properties in 2D c-CPs, and serving as a platform for integrating these materials into the currently available library of 2D materials.

Results and discussion

Sample preparation and characterization

Single-layer Cu_3BHT (Figure 1.a) was synthesized on the water surface using the Langmuir-Blodgett assisted method [13]. The synthetic procedure involved 3 steps: In step 1, 50 μl BHT solution (0.3 mg ml^{-1}) in chloroform/dimethylformamide (2:1, v/v) was spread on the water surface. After 10 min, the surface was compressed with a pair of Delrin barriers until the mean molecular area reached ~9.5 $Å^2$ (step 2), indicating the formation of tightly packed BHT molecules lying flat on the water surface. In step 3, 5 ml $Cu(NO_3)_2$ aqueous solution (1 mg ml^{-1}) was injected into the water subphase to initiate coordination polymerization for 5 h, affording a macroscopically homogeneous film with a lateral size of ~ 50 cm^2, a thickness of 0.8 nm and a root mean square (RMS) roughness of 0.1 nm (Figure S1 and Figure 1.b). Due to its reasonable electrical conductivity [13][14], and the absence of hydrogen, Cu_3BHT offers high stability under electron irradiation, which allows further investigation of its crystal structure by selected-area electron diffraction (SAED) and aberration-corrected high-resolution transmission electron microscopy (AC-HRTEM) [14] (see Figures 1.c and d). As shown in Figure 1.c, the SAED pattern of single-layer Cu_3BHT film displays sharp arcs with the nearest reflections at 1.37 nm^{-1}, which

corresponds to a *d* spacing of 0.73 nm. The AC-HRTEM image (Figure 1.d) reveals a highly ordered Kagome structure of Cu_3BHT with an atomic resolution of 1.2 Å. These results indicate the polycrystalline nature of single-layer Cu_3BHT film with a detectable domain size of tens of nm. Scanning transmission electron microscopy-energy dispersive X-ray spectroscopy and scanning electron microscopy with energy dispersive X-ray spectroscopy mapping analysis on the microscopic and macroscopic scale, respectively, demonstrates the uniform distribution of Cu, S, and C elements across the single-layer Cu_3BHT, confirming its compositional homogeneity and high quality. Surface-enhanced Raman spectroscopy (Figure S4), a highly sensitive technique for structural fingerprinting of ultrathin materials, reveals the disappearance of the -SH peak (~2512 cm^{-1}) in single-layer Cu_3BHT, indicating effective coordination between Cu and SH groups. The optical properties of single-layer Cu_3BHT were systematically investigated by ultraviolet-visible spectroscopy. As shown in Figure S5, single-layer Cu_3BHT exhibits substantial optical absorption, extending to 1600 nm, indicating a bandgap smaller than ~0.78 eV. This result reveals the semiconducting nature of single-layer Cu_3BHT.

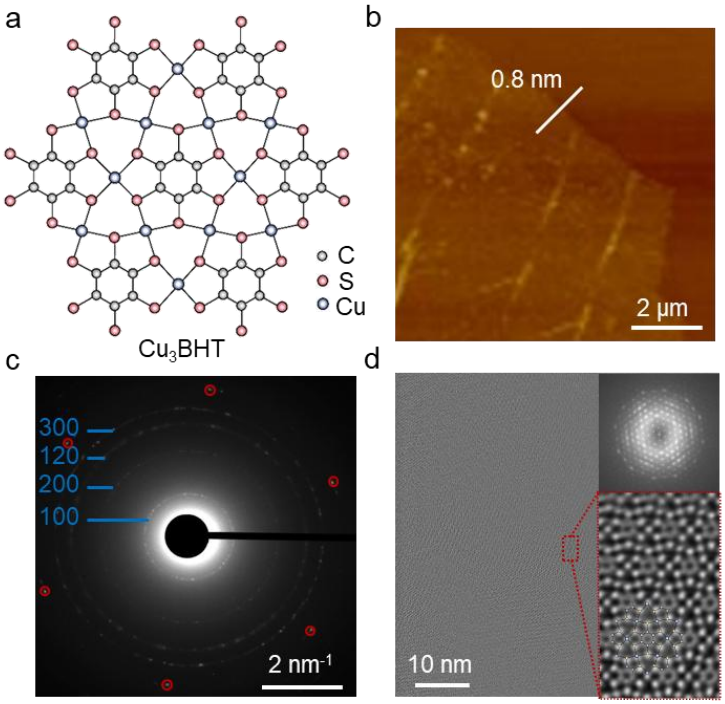

Figure 1. a. Schematic structure of Cu_3BHT. Cu, C, and S atoms are shown in blue, grey, and red, respectively. **b.** AFM image and height profile of single-layer Cu_3BHT. **c.** SAED pattern of Cu_3BHT.To mitigate the electron radiation-induced knock-on damage and electrostatic charging, we employed graphene encapsulation to enhance radiation resistance. Outset diffraction spots marked in red correspond to graphene. **d.** AC-HRTEM image of Cu_3BHT denoised using Wiener filtering. Inset: corresponding FFT pattern (top) and the enlarged AC-HRTEM image of the highlighted area (bottom).

Electrical characterization

The monolayer Cu_3BHT samples were transferred onto SiO_2/Si substrates by the horizontal dipping method. In a first attempt for characterizing the samples electrically, a post-photolithography step was used for defining metallic electrodes onto the Cu_3BHT. However, after this process we found that the devices were highly insulating, with responses well beyond our detection capabilities. Although more work is needed to rationalize this result, this observation might indicate a degradation of the electrical properties of the monolayer Cu_3BHT due to lithography processing. Therefore, we opted for a fabrication method not requiring any device fabrication processes after the single-layer was placed onto the SiO_2/Si substrate. To this end, substrates with pre-patterned Au/Ti-based contacts arranged in different device motifs were employed (see Supplementary Figures S6 and S7). We found this approach to be successful providing ohmic responses across the sample. To ensure that the current flowed through the Cu_3BHT and did not leak into the Si substrate, we measured the gate current. The results indicate that there was no significant leakage through the SiO_2 (see Supplementary Figure S9).

The first electrical characterization aimed at establishing the degree of homogeneity in terms of electrical response for the developed single-layer samples over an area of ~1cm^2. For that purpose, we measured the resistance by the 2-probe method with a metal pad contact separation of 50 μm at eight different locations evenly distributed across the 8 × 8 mm^2 sample area. We found ohmic responses in all the cases with a mean value of 53.29 kΩ and a maximum dispersion of 6% (see Supplementary Figures S10 and S11). These results demonstrated a good homogeneity in the electrical response for the studied single-layer sample within technologically relevant areas as large as 1 cm^2.

After characterizing the electrical response across the whole sample, we determined the contact resistance for the Cu_3BHT single-layer employing the transfer length method (TLM) (see insert of Figure 2.b for measurement configuration). Figure 2.a shows current-voltage characteristics for different distances between contact pads, *d*. An ohmic response was obtained in all the measurements with a value for the resistance increasing with *d*. From linear fits to the data, we obtained resistance values as summarized in Figure 2.b, revealing a linear dependence of resistance with the distance between probed electrodes. A linear fit to the data in Figure 2.b allows us to extract the contact resistance by extrapolating the linear curve to $d = 0$. The contact resistance was found to be 20.7 ± 1.5 kΩ; a figure that is commensurate with the resistance of the samples for the motifs employed here, with electrodes typically separated by 50 μm. This result highlights the eventual impact of the contact resistance on estimating the intrinsic conductivity of Cu_3BHT samples by the 2-probe method. To further investigate the potential impact of contact resistance on our measurements, we compared the resistance using the 2-probe and 4-probe methods at room

temperature (RT). We found that the 2-probe resistance (42.95 kΩ) was approximately an order of magnitude higher than the 4-probe resistance (6.12 kΩ) for a channel length of 50 µm between voltage probes. In addition, we investigated the temperature dependence of the contact resistance; the results suggested that the contact resistance barely changes with temperature over the analyzed T range (see Supplementary Figures S12 and S13).

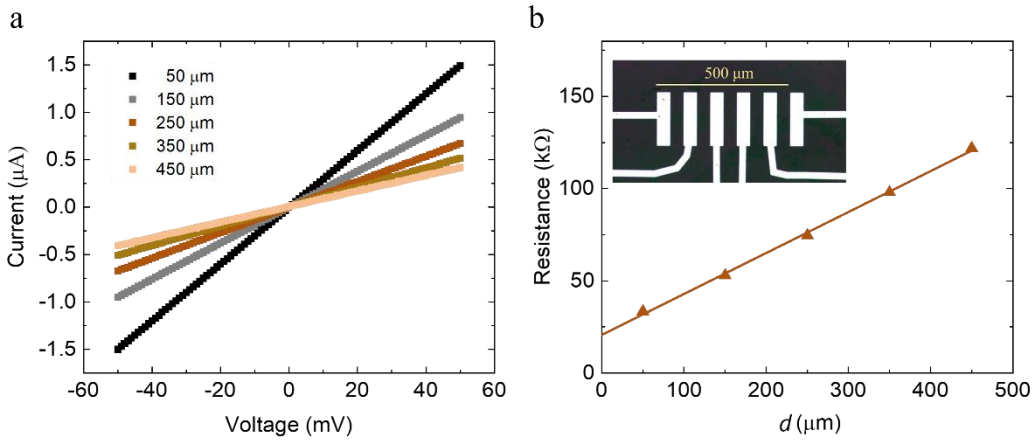

Figure 2. a. Current-voltage (I-V) characteristic of single-layer Cu_3BHT 2D c-CPs exhibiting ohmic behavior for different electrode separations. **b.** Resistance vs electrode separation, *d*, for single-layer Cu_3BHT samples for determining the contact resistance (R_C).

Next, the resistance´s temperature dependence was measured by the 4-probe method in order to ascertain the nature of charge transport in the single-layer samples. Initially, to prevent any eventual thermal damage, the sample was cooled from 300 K to 200 K. The resistivity vs temperature exhibited a behavior consistent with a semiconducting response, i.e. the resistivity increased as the temperature decreased, see Fig. 3 [15]. In a second cooling ramp we reached ~80 K, where a sharp increase of resistivity was observed. From that point, the sample was heated up to room temperature but the initial resistance value was not recovered. During subsequent warming-cooling cycles between 300 K and 4 K, a clear hysteresis in the resistivity curves was observed, and the initial recorded room temperature resistivity of 2 mΩ cm was not ever recovered. The different sharp jumps shown in the resistivity vs temperature curves (see Figure 3.a) indicate most likely that the current was following along different paths as the sample went through structural changes caused by the temperature sweeps [16]. This process might promote the formation of distinct percolation paths for the current as a function of temperature. After several cycles displaying hysteresis, the electrical behavior of single-layer Cu_3BHT settled to a state of reasonable stability and reproducibility. Once the sample provided a cooling-warming cycle free of hysteresis (Figure 3.b), the resistivity at room temperature was 10 mΩ cm, which is five times higher than the initial value (see Supplementary Figure S14). The observed variation in the room temperature resistivity during thermal cycling could be also due to an eventual

annealing process, where some contaminants are removed by the thermal treatment; more work is needed to ascertain this aspect.

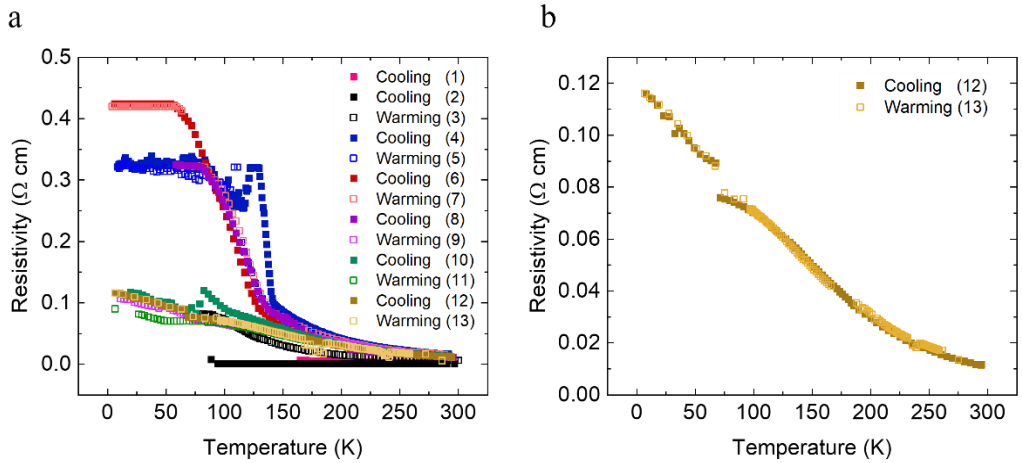

Figure 3. a. Resistivity-temperature of a single-layer Cu_3BHT sample during different temperature cycles. The numbers in parentheses indicate the order in which the measurements were conducted. The closed (open) symbols correspond to cooling (warming) temperature sweeps. **b.** Resistivity-temperature of single-layer Cu_3BHT MOF for cooling (12) and warming (13) temperature cycles once stabilization of the device resistance has been attained.

To further determine the nature of charge transport in the Cu_3BHT single-layer, we plotted the log of conductivity vs 1/T and $1/T^{1/3}$ as shown in Figures 4.a and 4.b, respectively. These representations serve the purpose of validating whether temperature-activated transport mechanisms linked to an Arrhenius-like (nearest-neighbor hopping model) or Mott variable range hopping-like (VRH) process are relevant. For the latter case we employed the VRH model considering a 2D system (the representation for a 3D model is given in the Supplementary Figure S15. b). We found that the experimental data could not be fitted by a single function over the whole probed T range for any of these two models; notably, a result in agreement with a previous work analyzing the same material in its bulk-like form [17]. Therefore, this result might imply the possible existence of different transport regimes as a function of T in the studied samples. However, while there are arbitrary temperature regions where a good fit could be obtained for any of these two transport models, we found that a good linear fit of log(σ) vs T from 300 K to 125 K was able to describe de data properly (see Figure 4.c); this T fitting range was much larger than any other considering either a simple Arrhenius-like or VRH-like model (see Figure 4). This type of exponential dependence of the conductivity has been previously observed in inorganic [12] and organic [18][19] semiconductor samples displaying modest mobilities. In all the cases, the log(σ) vs T linear dependence can be ascribed to a temperature-dependent tunneling process

controlling the conduction mechanism in the samples [12]. Within this model, in simple terms, the tunneling barrier has a vibrating width. As the T is increased, tunneling must eventually turn into hopping as electrons should acquire enough energy to surmount the barrier. On the contrary, for low enough temperatures, the barrier will reach its zero-point energy providing a flat temperature-independent conductivity. The latter observation could be consistent with the collected experimental data below and until 50K where the sample levels off till suffering a reproducible jump to another quasilinear region (see Figure 3.b and Supplementary Figure S15). By comparing different models over the same large available temperature window, we conclude that the most plausible scenario governing charge transport in the analyzed Cu_3BHT single-layer samples is tunneling between localized states with a thermally induced overlap.

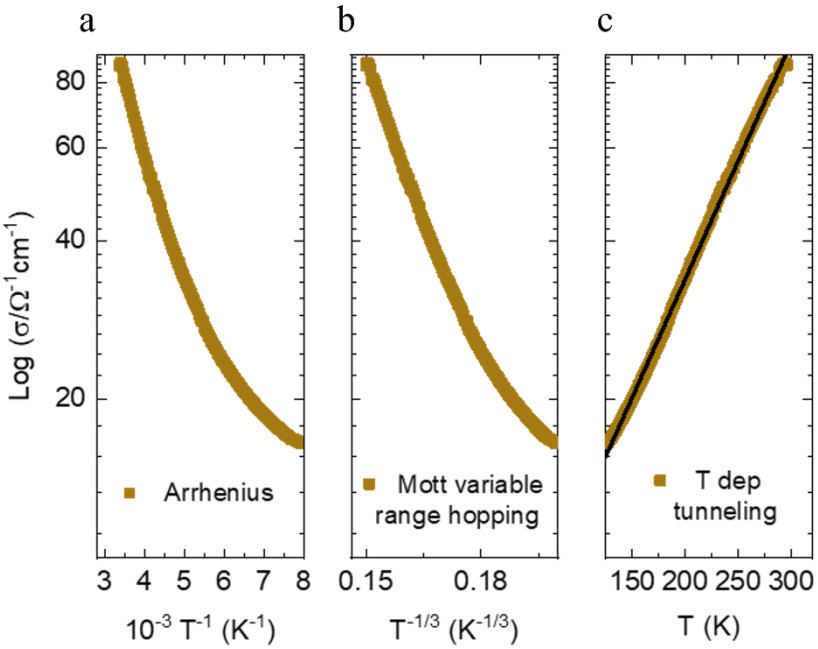

Figure 4. Log of conductivity vs **a.** 1/T (Arrhenius), **b.** $1/T^{1/3}$ (2D Mott variable-range hopping) and **c.** T (T-dependent tunneling) from 300 K to 125 K.

As summarized above, the measured Cu_3BHT single-layer exhibited a temperature-activated semiconductor-like behavior. Furthermore, a T-dependent tunneling charge transport evidenced by a log(σ) vs T linear dependence is characteristic of a low-mobility semiconductor. Notably, these observations seem to be at odds with several previous theoretical [20] and experimental [10] reports that supported the metallic nature of this type of MOF in their single-layer and van der Waals (vdW) stack forms (but resolved experimentally only on bulk-like vdW stack samples). In these previous works, it was rationalized a T dependent semiconducting-like behavior arguing that thermally activated transport was a consequence of the polycrystalline nature of the samples [21][22] (i.e. grains are metallic, but potential barriers at grain boundaries cause an increase in

the overall sample resistance). This behavior has indeed been claimed for 2D c-MOFs before [23][24] and is common in polycrystalline inorganic-based samples [25][26]. On the other hand, our results are in agreement with a recent report claiming semiconducting-like behavior for single-layer Cu_3BHT coupled to graphene [13]. We performed VB-XPS characterization on a region with no metal contacts for the same sample as the one reported in Figure 3 (see Supplementary Figure S16). Our results show a response that could indeed be consistent with a semiconducting behavior (see Supplementary Figure S17).

Theoretical calculations

Due to the disparity of results reported regarding the metallic (gapless) or semiconducting (gapped) nature of the samples studied herein we have reevaluated the DFT calculations to study Cu_3BHT single-layer electronic structure in more detail. We have found that when we have used the standard atomistic model of flat Cu_3BHT (Figure 5.a), used previously [27], we obtained that its phonon spectrum exhibits imaginary frequencies and thus a flat self-standing Cu_3BHT single-layer is not a stable structure (Figure 5.b). Instead, the standalone Cu_3BHT single-layer has an inherently wavy structure with a periodicity of 2×2 Cu_3BHT unit cells, wavy along both *a* and *b* lattice vectors (Figure 5.d, e). Notably, this structure is 0.87 eV per Cu_3BHT more stable than the flat configuration. While the flat Cu_3BHT structure is well established to be metallic (Figure 5.c), the wavy structure is instead semiconducting with a band gap of 1.4 eV (Figure 5.e). However, in a recent study it was argued that when Cu_3BHT is deposited on a flat surface, it should assume a flat geometry [13], and hence have a metallic character according to theory. Furthermore, we have included solvent molecules in the DFT calculations and found that water molecules – present during sample synthesis - interact strongly with the Cu_3BHT surface (see Supplementary Information). The interaction with water might reinforce the driving force for Cu_3BHT to be wavy and at high surface coverage would eventually cause it to be wavy even when deposited onto a substrate. This might indeed introduce a band gap in the sample, which would eventually disappear if water is removed (Supplementary Figure S18). While these theoretical results suggest some scenarios that might rationalize the apparent semiconducting, rather than metallic, nature of the samples studied herein, it is clear that more combined experimental and theoretical work is needed to elucidate this basic and fundamental aspect.

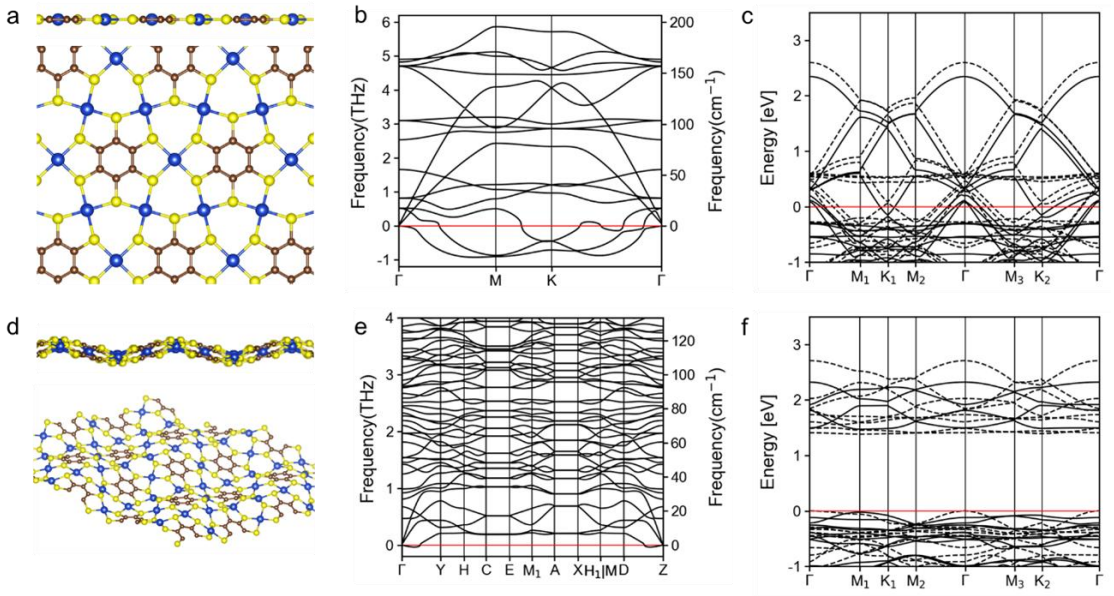

Figure 5. a. Crystalline structure, **b.** phonon spectrum and **c.** band structure of flat Cu_3BHT single-layer. **d.** Structure, **e.** phonon spectrum and **f.** band structure of wavy Cu_3BHT single-layer. Wavy single-layer unit cell consists of four Cu_3BHT structural units. Full and dashed lines in the band structure denote spin up and spin down bands. High-symmetry k-points and path in the Brillouin zone are shown in Supplementary Figure S18.

Conclusions

In this work, we report the production and electrical characterization of large-area single-layers of Cu_3BHT synthesized on the water surface using the Langmuir-Blodgett method. Electron diffraction and HRTEM show that the samples are polycrystalline. The electrical characterization showed ohmic responses across areas as large as $1cm^2$ with a mean value of ~53 ± 3 kΩ (50 μm probe separation). Cooling and heating sweeps revealed hysteresis on the electrical response, suggesting that the current followed different paths as the sample underwent structural changes induced by temperature variations and possible desorption of contaminants during temperature cycling. After a few cycles, the hysteresis vanished and the electrical response was characterized by a linear log(σ) vs T response (from 300 K to 125 K). This final stable behavior can be attributed to a temperature-dependent tunneling process governing the conduction mechanism in the single-layer Cu_3BHT with a polycrystalline nature; an observable reported previously for low mobility semiconductors. These results, together with DFT studies and VB-XPS data point in the direction of a semiconducting (gapped) rather than metallic (gapless) nature of the samples studied here. However, more work is clearly needed to fully determine the relationship between structure and macroscopic properties in this 2D material. In the future, it will also be critical to deepen the understanding of charge transport mechanisms in single-layers, ideally on single crystalline ones.

Finally, taking into account the lessons learned from other 2D systems, analyzing the impact of substrate on electrical properties as well as any eventual semiconducting-to-metallic transitions on vdW stacked samples are also important.

Methods

Synthesis of single-layer Cu_3BHT

The single-layer Cu_3BHT was synthesized on the water surface of a Langmuir–Blodgett through (KSV NIMA), which was equipped with a platinum Wilhelmy plate, a Taflon dipper, and a pair of Delrin barriers. During the synthesis, 50 μL of BHT solution (0.3 mg mL^{-1}) in chloroform/dimethylformamide (2:1, v/v) was spread on the water surface with a microsyringe. The solvent was allowed to evaporate for 30 min and then the compression was carried out by the barriers at a rate of 2 mm min^{-1} until the surface pressure reached 10 mN m^{-1}. Then, 5 mL $Cu(NO_3)_2$ aqueous solution (1 mg mL^{-1}) was injected into the water subphase to initiate the coordination polymerization. After 5 h, the synthetic single-layer Cu_3BHT film was deposited onto the substrates by the horizontal dipping method. The samples were immersed in Milli-Q water for 5 min, rinsed with flowing ethanol and acetone, and then dried at 80 °C.

Structural characterization

Optical microscopy and AFM images were recorded on a 300 nm SiO_2/Si substrate. TEM experiments were performed on an image-side spherical and chromatic aberration-corrected Sub-Ångström Low-Voltage Electron Microscope (SALVE) instrument at 80 kV. The SALVE Cs/Cc corrector adopts a quadrupole-octupole design, which corrects the geometrical axial aberrations up to the 5rd-order, off-axial aberrations up to the 3rd order, and chromatic aberration. Data acquisition was conducted on a Ceta CMOS camera. We employed an electron dose rate of ~0.6 e-/$Å^2$s when searching for the region of interest (ROI). An objective aperture was inserted to enhance the image contrast in searching mode. The setting of sampling, dose rate, and defocus, was conducted in the vicinity of ROI. The acquisition dose for Cu_3BHT is 3.2×103 e^- $Å^{-2}$ (at 80 kV, pixel size: 0.15 Å). The image simulation is conducted by QSTEM1, simulation conditions: thickness single-layer of Cu_3BHT (crystal information based on DFT calculation), defocus 6 nm.

DFT calculations

Phonon calculations of the single-layer Cu_3BHT were carried out using FHI-aims [28][29] program with FHI-vibes [30] package for vibrational properties of solids. All structures were fully optimized (atom positions and lattice parameters) with PBE [31] functional and tight tier 1 [28] basis set, using Tkatchenko-Scheffler dispersion correction [32] and Γ-centered k-grids of 12×12×1. For phonon band structure calculation, k-grids of 3×3×1, and 2×2×1 are used for 1×1

unit cell Cu_3BHT (flat structure) and 2x2 unit cell Cu_3BHT (wavy structure), respectively. The phonon calculation in FHI-vibes were performed using the finite displacement method and finite supercell of 3×3×1.

Band structure and water adsorption calculations were carried out using CRYSTAL17 [33][34] program package. All the structures were fully optimized (atom positions and lattice parameters) with PBE0 [35] exchange-correlation functional with D3 [36][37] dispersion correction and POB-TZVP (rev2) [38] basis set. A k-point grid of 12×12×1 was employed for final structural optimizations and electronic structure. The spin state was optimized in all calculations, with final spin state close to the S = 1 per Cu_3BHT structural unit. All DFT calculations reported in this work are available in the NOMAD online repository under the DOI:[will be added during the revision process].

Device fabrication

Device´s fabrication process took place in a cleanroom facility, at the Centre of Micro and Nanofabrication of IMDEA Nanoscience. The samples were deposited onto a low-resistivity (<0.05 Ω cm) silicon wafer, capped with a 290 nm thermally-grown silicon oxide layer. Different contact array geometries as explained in the Supplementary information were made using maskless UV laser lithography, followed by evaporation of titanium and gold (20 and 80 nm, respectively) in an electron beam system at ultra-high vacuum (10^{-8}-10^{-9} mbar). After evaporation, a lift-off was performed in acetone at 50 °C for 1 h. After this, a gentle isopropanol rinse and N_2 drying process was carried out. These pre-patterned substrates were used for fabricating devices using the Route 1 as described in the Supplementary Information.

Electrical characterization

A wire bonder HB10 was employed to establish interconnections between the Au pads on the samples and the sample holder using Au wires (see Supplementary Information for the parameters used). Current voltage (I-V) measurements were done in a cleanroom environment with a temperature of 293.15 K, atmospheric pressure, and humidity of 50% using an Everbeing manual probe station, not connected electrically to the ground, has been utilized to measure the resistance of the devices at ambient conditions using 2- and 4-probe methods. We used the technique of measuring with both positive and negative current to eliminate thermal voltages, known as the Reverse DC Technique or Delta Mode. The resistance was calculated using the Ohm's law, $R = V/I$.

While the sample was not measured, we keep it stored in a desiccator to prevent deterioration. The resistance vs temperature measurements were done in an Oxford Optistat AC-V12 closed-cycle helium cryostat, under a pressure on the order of 10^{-5} mbar. The resistance was measured

by a Keithley 2450 source-meter using DC current and the temperature was controlled by means of an Oxford 350 temperature controller. A current of 10 μA was applied between the first and fourth pads, and the voltage was measured between the second and third pads, obtaining the resistance for a 50 μm separation, from these data, the resistivity can be calculated using the relation: $\rho = (A/d)\,R$, where A represents the area perpendicular to the current flow, and d denotes the distance between the voltage electrodes.

Supplementary Information

The supplementary information contains details about synthesis, description of instruments, experimental characterization, theoretical modeling and conductivity measurements.

Acknowledgments

This contribution has been made within the project EMPIR 20FUN03 COMET *Two dimensional lattices of covalent- and metal-organic frameworks for the Quantum Hall resistance standard,* financed by the *European Metrology Programme for Innovation and Research* (EMPIR), co-financed by the participating states and the research and innovation program of the European Union, Horizon 2020. T.L., M.P. and T.H. thank ZIH Dresden and Paderborn Center for Parallel Computing (PC^2) for the use of computational resources. Z. W., R.D. and X.F. thank ERC starting grant (FC2DMOF, No. 852909) and SPP 2244 (2DMP). R.D. thanks National Natural Science Foundation of China (22272092), Taishan Scholars Program of Shandong Province (tsqn201909047) and the Natural Science Foundation of Shandong Province (ZR2023JQ005). T.L. and T.H. thank the CRC 1415 (Chemistry of Synthetic Two-Dimensional Materials, No. 417590517). S.M.E. and G.C. thank their fellowships provided by the Community of Madrid (PIPF-2022TEC-24849 and PIPF-2022TEC-24324). I.F.C. and J.G.P. thank their FPI fellowships from AEI-MCIN (PRE2020-092625 and PRE2022-102081). E.C. acknowledges funding from Spanish Project - CNS2022-136203 - Consolidación investigadora. The authors acknowledge Dr. Baokun Liang, Prof. Ute Kaiser, and Prof. Inez M. Weidinger for HRTEM, STEM-EDS, and surface-enhanced Raman measurements.

References

[1] R. Dong., H. Arora, M. Ballabio, M. Karakus, Z. Zhang, C. Shekhar, P. Andler, P. St, Petkov, A. Erbe, S. C. B. Mannsfeld, C. Felser, T. Heine, M. Bonn, X. Feng, E. Cánovas. *Nat. Mater*. **2018**, 17, 1027.

[2] J. H. Dou, M. Q. Arguilla, Y. Luo, J. Li, W. Zhang, L. Sun, J. L. Mancuso, L. Yang, T. Chen, L. R. Parent, G. Skorupskii, N. J. Libretto, C. Sun, M. C. Yang, P. V. Dip, E. J. Brignole, J. T. Miller, J. Kong, C. H. Hendon, J. Sun, M. Dinkă. *Nat. Mater.* **2021**, 20, 222-228.

[3] M. Wang, R. Dong, X. Feng. *Chem. Soc. Rev*. **2021**, 50, 2764-2793.

[4] L. Sun, B. Liao, D. Sheberla, D. Kraemer, J. Zhou, E. A. Stach, D. Zakharov, V. Stavila, A. A. Talin, Y. Ge, M. D. Allendorf, G. Chen, F. Léonard, M. Dinkă. *Joule* **2017**, 1, 168.

[5] T. Kambe, R. Sakamoto, T. Pal, N. Fukui, K. Hoshiko, T. Shimojima, Z Wang, T. Hirahara, K. Ishizaka, S. Hasegawa, F. Liu, H. Nishihara. *J. Am. Chem. Soc.* **2014**, 136, 41, 14357-14360.

[6] M. Ko, L. Mendecki, K. A. Mirica, *Chem.Commun.* **2018**, 54, 7873–7891.

[7] R. W. Day, D. K. Bediako, M. Rezaee, L. R. Parent, G. Skorupskii, M. Q. Arguilla, C. H. Hendon, I. Stassen, N. C. Gianneschi, P. Kim, M. Dinkă. *ACS Cent. Sci*. **2019**, 5, 1959−1964.

[8] X. Huang, S. Zhang, L. Liu, L. Yu, G. Chen, W. Xu, D. Zhu. *Angew. Chem., Int.* **2018**, 57, 146−150.

[9] R. K. Parashar, P. Jash, P. C. Mondal **2022**. Metal-Organic Frameworks in Semiconductor Devices: Recent Advancements and a Bright Future. *arXiv preprint arXiv:*2206.13473.

[10] X. Huang, P. Sheng, Z. Tu, F. Zhang, J. Wang, H. Geng, Y. Zou, C. Di, Y. Yi, Y. Sun, W. Xu, D. Zhu. *Nat Commun.* **2015**, 6, 7408.

[11] Z. Wang, L. S. Walter, M. Wang, P. St. Petkov, B. Liang, H. Qi, N. N. Nguyen, M. Hambsh, H. Zhong, M. Wang, S. Park, L. Renn, K. Watanabe, T. Taniguchi, S. C. B. Mannsfeld, T. Heine, U. Kaiser, S. Zhou, R. T. Weitz, X. Feng, R. Dong. *J. Am. Chem. Soc.* **2021**, 143, 34, 13624-13632.

[12] C. M. Hurd. *J. Phys. C. Solid State Phys*. **1985**, 18, 6487.

[13] Z. Wang, S. Fu, W. Zhang, B. Liang, T. J. Liu, M. Hambsh, J. F. Pöhls, Y. Wu, J. Zhang, T. Lan, X. Li, H. Qi, M. Polozij, S. C. B. Mannsfeld, U. Kaiser, M. Bonn, R. T. Weitz, T. Heine, S. S. P. Parkin, H. I. Wang, R. Dong, X. Feng. *Adv. Mater.* **2024**, 2311454.

[14] D. Mücke, I. Cooley, B. Liang, Z. Wang, S. Park, R. Dong, X. Feng, H. Qi, E. Besley, U. Kaiser. *Nano Lett.* **2024**, 24, 10, 3014–3020.

[15] R. A. Butera, D. H. *J. Waldeck. Chem. Educ.* **1997**, 74, 9, 1090.

[16] F. X. Coudert. *Chem. Mater.* **2015**, 27, 6, 1905–1916.

[17] R. Tsuchikawa, N. Lotfizadeh, N. Lahiri, S. Liu, M. Lach, C. Slam, J. Louie, V. V. Deshpande. *Phys. Status Solidi A.* **2020**. 217, 23, 2000437.

[18] D. R. Stewart, D. A. A. Ohlberg, P. A. Beck, C. N. Lau, R. S. Williams. *Appl. Phys. A.* **2005**, 80, 1379-1383.

[19] C. N. Colesniuc, R. R. Biswas, S. A. Hevia, A. V. Balatsky, I. K. Schuller. *Phys. Rev. B* **2011**, 83, 085414.

[20] X. H. Bu, M. J. Zaworotko, Z. Zhang. Metal-Organic Framework from design to application. *Springer*. **2020**.

[21] G. Reiss, J. Vancea, H. Hoffmann. *Phys. Rev. Lett.* **1985**. 56, 19.

[22] A. M. van der Zande, P. Y. Huang, D. Chenet, T. C. Berkelbach, Y. You, G. H. Lee, T. F. Heinz, D. R. Reichman, D. A. Muller, J. C. Hone. *Nature Mater.* **2013**. 12, 554–561.

[23] X. Song, J. Liu, T. Zhang, L. Chen. *Sci. China Chem.* **2020**, 63, 1391–1401.

[24] E. M. Johnson, S. Ilic, A. J. Morris. *ACS Cent. Sci*. **2021**, 7, 445-453.

[25] S. Hamada, K. Kawahara, S. Tsurekawa, T. Watanabe, T. Sekiguchi. *MRS Proceedings* **1999**, 586, 163.

[26] H. F. Mataré. *J. Appl. Phys*. **1984**, 56, 2605-2631.

[27] X. Zhang, Y. Zhou, B. Cui, M. Zhao, F. Liu. *Nano Lett.* **2017**, 17, 10, 6166–6170.

[28] V. Blum, R. Gehrke, F. Hanke, P. Havu, V. Havu, X. Ren, K. Reuter, M. Scheffler. *Comput. Phys. Commun.* **2009**. 180**,** 2175-2196.

[29] X. Ren, P. Rinke, V. Blum, J. Wieferink, A. Tkatchenko, A. Sanfilippo, K. Reuter, M. Scheffler. *New Journal of Physics* **2012**. 14, 053020.

[30] F. Knoop, T. A. R. Purcell, M. Scheffler, C. Carbogno. *J. Open Source Softw* **2020.** 5(56), 2671.

[31] J. P. Perdew, K. Burke, M. Ernzerhof. *Phys. Rev. Lett.* **1996.** 77, 3865.

[32] A. Tkatchenko, M. Scheffler. *Phys. Rev. Lett.* **2009.** 102**,** 073005.

[33] R. Dovesi, A. Erba, R. Orlando, C. M. Zicovich-Wilson, B. Civalleri, L. Maschio, M. Rérat, S. Casassa, J. Baima, S. Salustro, B. Kirtman. *Rev. Comput. Mol. Sci.* **2018.** 8**,** e1360.

[34] R. Dovesi, V. R. Saunders, C. Roetti, R. Orlando, C. M. Zicovich-Wilson, F. Pascale, B. Civalleri, K. Doll, N. M. Harrison, I. J. Bush, Ph. D´arco, M. Llunel, M. Causà, Y. Noël, L. Maschio, A. Erba, M. Rérat, S. Casassa. CRYSTAL17 **2017**.

[35] C. Adamo, V. Barone. *J. Chem. Phys.* **1999.** 110, 6158-6170.

[36] S. Grimme, J. Antony, S. Ehrlich, H. Krieg. *J. Chem. Phys.* **2010.** 132**,** 154104.

[37] S. Grimme, S. Ehrlich, L. Goerigk. *J. Comput. Chem.* **2011.** 32**,** 1456-1465.

[38] D. V. Oliveira, J. Laun, M. F. Peintinger, T. Bredow. *J. Comput. Chem.* **2019.** 40, 2364-2376.